

# Infrared spectroscopy of cataclysmic variables: III. Dwarf novae below the period gap and novalike variables

V. S. Dhillon<sup>1</sup>, S. P. Littlefair<sup>1</sup>, S. B. Howell<sup>2</sup>, D. R. Ciardi<sup>3</sup>, M. K. Harrop-Allin<sup>4</sup>  
and T. R. Marsh<sup>5</sup>

<sup>1</sup>*Department of Physics and Astronomy, University of Sheffield, Sheffield S3 7RH, UK*

<sup>2</sup>*Astrophysics Group, Planetary Science Institute, 620 North 6<sup>th</sup> Ave., Tuscon, AZ 85705, USA*

<sup>3</sup>*Department of Astronomy, 211 Bryant Space Sciences Building, University of Florida, Gainesville, FL 32611, USA*

<sup>4</sup>*Mullard Space Science Laboratory, University College London, Holmbury St. Mary, Dorking, Surrey RH5 6NT, UK*

<sup>5</sup>*Department of Physics and Astronomy, University of Southampton, Highfield, Southampton SO17 1BJ, UK*

Accepted for publication in the Monthly Notices of the Royal Astronomical Society

13 July 2021

## ABSTRACT

We present K-band spectra of the short-period dwarf novae YZ Cnc, LY Hya, BK Lyn, T Leo, SW UMa and WZ Sge, the novalike variables DW UMa, V1315 Aql, RW Tri, VY Scl, UU Aqr and GP Com, and a series of field dwarf stars with spectral types ranging from K2–M6.

The spectra of the dwarf novae are dominated by emission lines of H I and He I. The large velocity and equivalent widths of these lines, in conjunction with the fact that the lines are double-peaked in the highest inclination systems, indicate an accretion disc origin. In the case of YZ Cnc and T Leo, for which we obtained time-resolved data covering a complete orbital cycle, the emission lines show modulations in their equivalent widths which are most probably associated with the bright spot (the region where the gas stream collides with the accretion disc). There are no clear detections of the secondary star in any of the dwarf novae below the period gap, yielding upper limits of 10–30% for the contribution of the secondary star to the observed K-band flux. In conjunction with the K-band magnitudes of the dwarf novae, we use the derived secondary star contributions to calculate lower limits to the distances to these systems.

The spectra of the novalike variables are dominated by broad, single-peaked emission lines of H I and He I – even the eclipsing systems we observed do not show the double-peaked profiles predicted by standard accretion disc theory. With the exception of RW Tri, which exhibits Na I, Ca I and <sup>12</sup>CO absorption features consistent with a M0V secondary contributing 65% of the observed K-band flux, we find no evidence for the secondary star in any of the novalike variables. The implications of this result are discussed.

**Key words:** binaries: close – stars: individual: YZ Cnc, LY Hya, BK Lyn, T Leo, SW UMa, WZ Sge, DW UMa, V1315 Aql, RW Tri, VY Scl, UU Aqr, GP Com – novae, cataclysmic variables – infrared: stars

## 1 INTRODUCTION

Cataclysmic variables (CVs) are interacting binary systems in which a white dwarf primary accretes material from a red dwarf secondary (see Warner 1995 for a review). The infrared (IR) is a relatively unexplored part of the spectrum as far as CVs are concerned (see Dhillon 1998 for a

review). This is suprising given the fact that the 1–2.5  $\mu$ m wavelength range happens to be where spectrum of the G–M-dwarf secondary star in CVs is expected to peak<sup>\*</sup>, and

<sup>\*</sup> The spectral type of the secondary star in a CV can be determined from its orbital period,  $P$ , using the relationships

where low-harmonic, cyclotron emission from the weaker-field magnetic CVs and emission from the cool, outer regions of the accretion disc in non-magnetic CVs would be expected to fall. For the above reasons, we embarked on a spectral survey of CVs in the IR, the results of which have been published in Dhillon & Marsh (1995: Paper I – dwarf novae above the period gap) and Dhillon et al. (1997: Paper II – intermediate polars).

Two of the types of CV which were not surveyed in Papers I and II were the dwarf novae below the period gap and the novalike variables. These represent the two classes of CV in which the secondary star has proved to be hardest to detect in optical spectra (e.g. Friend et al. 1988, Smith et al. 1997). In fact, table 1 of Smith & Dhillon (1998) shows that the secondary star has been directly observed in only 4 dwarf novae below the period gap and 4 novalike variables, compared to a total of 55 detections in all classes of CV. In the case of dwarf novae below the period gap, the paucity of secondary star detections is probably due to the fact that the secondary star is of a very late-type and hence faint. In the case of the novalike variables, the lack of secondary star detections is probably due to the very bright discs drowning out the light from the companion. If we are to learn anything about the secondary stars in these systems, and hence how these types of CV evolve, some means of detecting the secondary star must be found. Given that light from the disc should be relatively weak in the IR, and that the secondary star should peak in the IR, we decided to perform an IR spectral survey of dwarf novae below the period gap and novalike variables in order to detect their elusive secondary stars. The results of this survey are presented in this third and final paper in the series.

## 2 OBSERVATIONS

The data presented in this paper were obtained between 1993 February 8 and 1997 May 28 with the 1–5  $\mu\text{m}$  Cooled Grating Spectrometer 4 (CGS4) on the United Kingdom 3.8 m Infrared Telescope (UKIRT) on Mauna Kea, Hawaii. With the exception of GP Com, which was observed with the instrumental configuration described by Dhillon et al. (1997), all of the spectra presented in this paper were obtained with the  $256 \times 256$  pixel InSb array, the 75 l/mm grating in first order and the 150 mm camera, giving a wavelength range of approximately  $0.6 \mu\text{m}$  at a resolution of  $350 \text{ km s}^{-1}$ . Optimum spectral sampling and bad pixel removal were obtained by mechanically shifting the array over 2 pixels in the dispersion direction in steps of 0.5 pixels. We employed the non-destructive readout mode of the detector in order to reduce the readout noise. The slit width was 1.2 arcseconds (projecting to 1 pixel on the detector) and the slit was oriented at the parallactic angle. The seeing disc was usually equal to or slightly larger in size than the slit width, except on the night of 1997 May 28, when we employed

$26.5 - 0.7P$  (for  $P < 4 \text{ hr}$ ) and  $33.2 - 2.5P$  (for  $P > 4 \text{ hr}$ ), where  $G0=0$ ,  $K0=10$  and  $M0=20$  (Smith & Dhillon 1998). The wavelength,  $\lambda_{\text{max}}$ , of the peak flux,  $f_{\nu}$ , for a star of effective temperature  $T_{\text{eff}}$  can be approximated by:  $\lambda_{\text{max}} = 5100/T_{\text{eff}} \mu\text{m}$ . With  $T_{\text{eff}}$  ranging from  $\sim 6000$ – $2000 \text{ K}$  for the G–M-dwarf secondary stars in CVs,  $\lambda_{\text{max}}$  ranges from  $\sim 1$ – $2.5 \mu\text{m}$ .

the new tip-tilt secondary mirror to produce sub-arcsecond images. The observations were all obtained in photometric conditions, apart from the night of 1995 October 21 which suffered from a little high cirrus. In order to compensate for fluctuating atmospheric  $\text{OH}^-$  emission lines (Ramsay, Mountain & Geballe 1992) we took relatively short exposures and nodded the telescope primary so that the object spectrum switched between two different spatial positions on the detector. A full journal of observations is presented in table 1.

## 3 DATA REDUCTION

The initial steps in the reduction of the 2D frames were performed automatically by the CGS4 data reduction system (Daley & Beard 1994). These were: the application of the bad pixel mask, bias and dark frame subtraction, flat field division, interlacing integrations taken at different detector positions, and co-adding and subtracting nodded frames. Further details of the above procedures may be found in the review by Joyce (1992). In order to obtain 1D data, we subtracted the residual sky and then optimally extracted the spectra (Horne 1986).

There were three stages to the calibration of the spectra. The first was the calibration of the wavelength scale using argon arc-lamp exposures. The second-order polynomial fits to the arc lines always yielded an error of less than  $0.0003 \mu\text{m}$  (rms). The next step was the removal of the ripple arising from variations in the star brightness between integrations (i.e. at different detector positions). These variations were due to changes in the seeing, sky transparency and the slight motion of the stellar image relative to the slit. We discovered that the amplitude of the ripple varied across the spectrum and we were thus forced to apply a correction for this based on a linear interpolation of the ripple profiles at either end of the spectrum. The final step in the spectral calibration was the removal of telluric atmospheric features and flux calibration. This was performed by dividing the spectra to be calibrated by the spectrum of an F-type standard, observed at a similar airmass (typically within 0.1), with its prominent stellar features masked out. We then multiplied the result by the known flux of the standard at each wavelength, determined using a black body function set to the same temperature and magnitude as the standard. As well as providing flux calibrated spectra, this procedure also removed atmospheric absorption features from the object spectra.

## 4 RESULTS

Figure 1 shows the K-band spectra of the dwarf novae YZ Cnc, LY Hya, BK Lyn, T Leo, SW UMa and WZ Sge, and figure 2 shows the K-band spectra of the novalike variables GP Com, DW UMa, V1315 Aql, RW Tri, VY Scl and UU Aqr. Note that the anti-dwarf novae DW UMa and VY Scl were both in their high state when the spectra in figure 2 were obtained. In figure 3 we show the K-band spectra of main-sequence field dwarfs ranging in spectral type from K2 to M6 and in tables 2 and 3 we list the wavelengths,

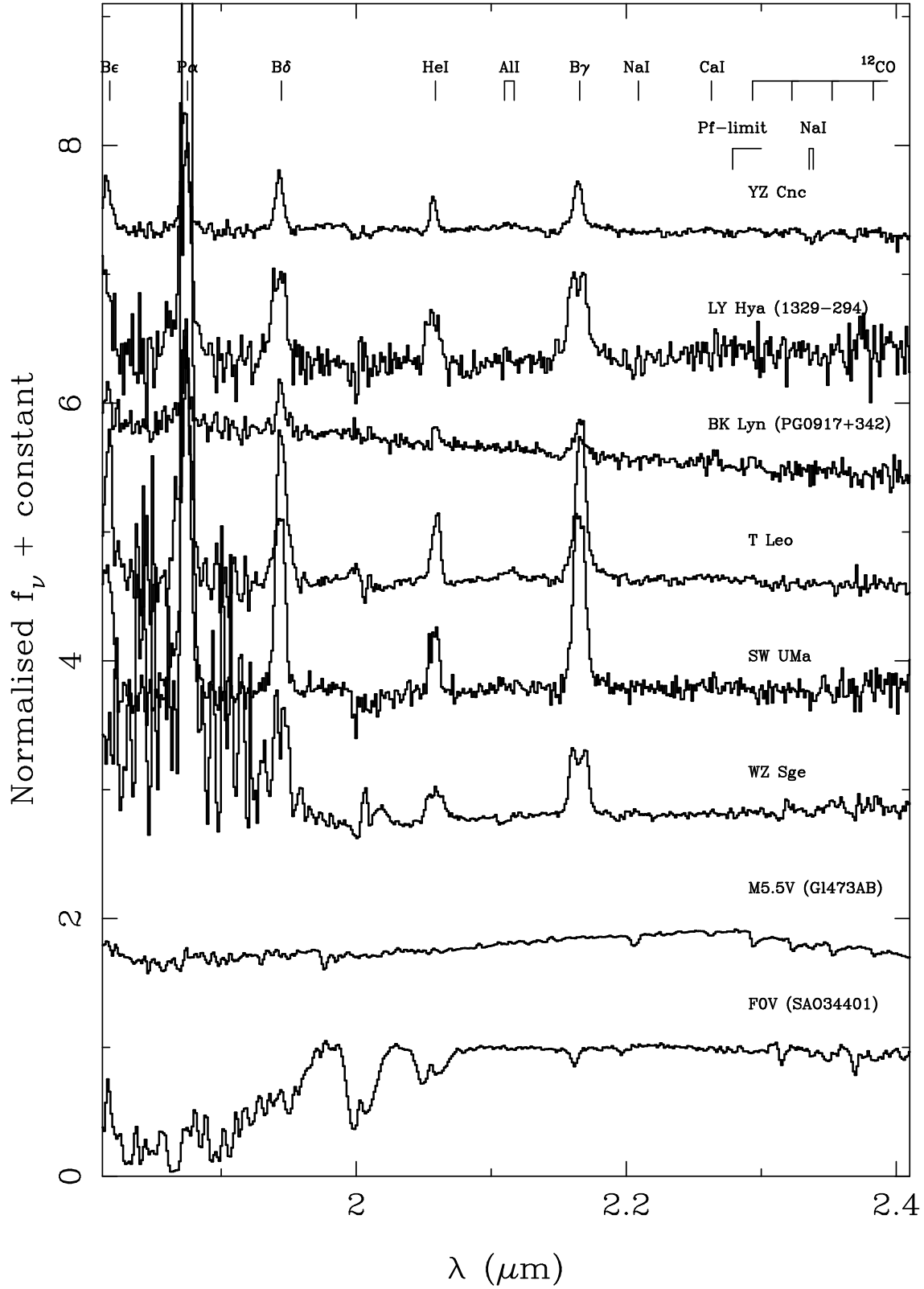


**Figure 1.** K-band spectra of the dwarf novae YZ Cnc, LY Hya, BK Lyn, T Leo, SW UMa, WZ Sge and an M5.5V star. The spectra have been normalised by dividing by the flux at  $2.24 \mu\text{m}$  and then offset by adding a multiple of 0.9 to each spectrum. Also shown is the spectrum of an F0V star, normalised by dividing by a spline fit to its continuum, which indicates the location of telluric absorption features; spectral features within the strongest absorption bands are highly uncertain.

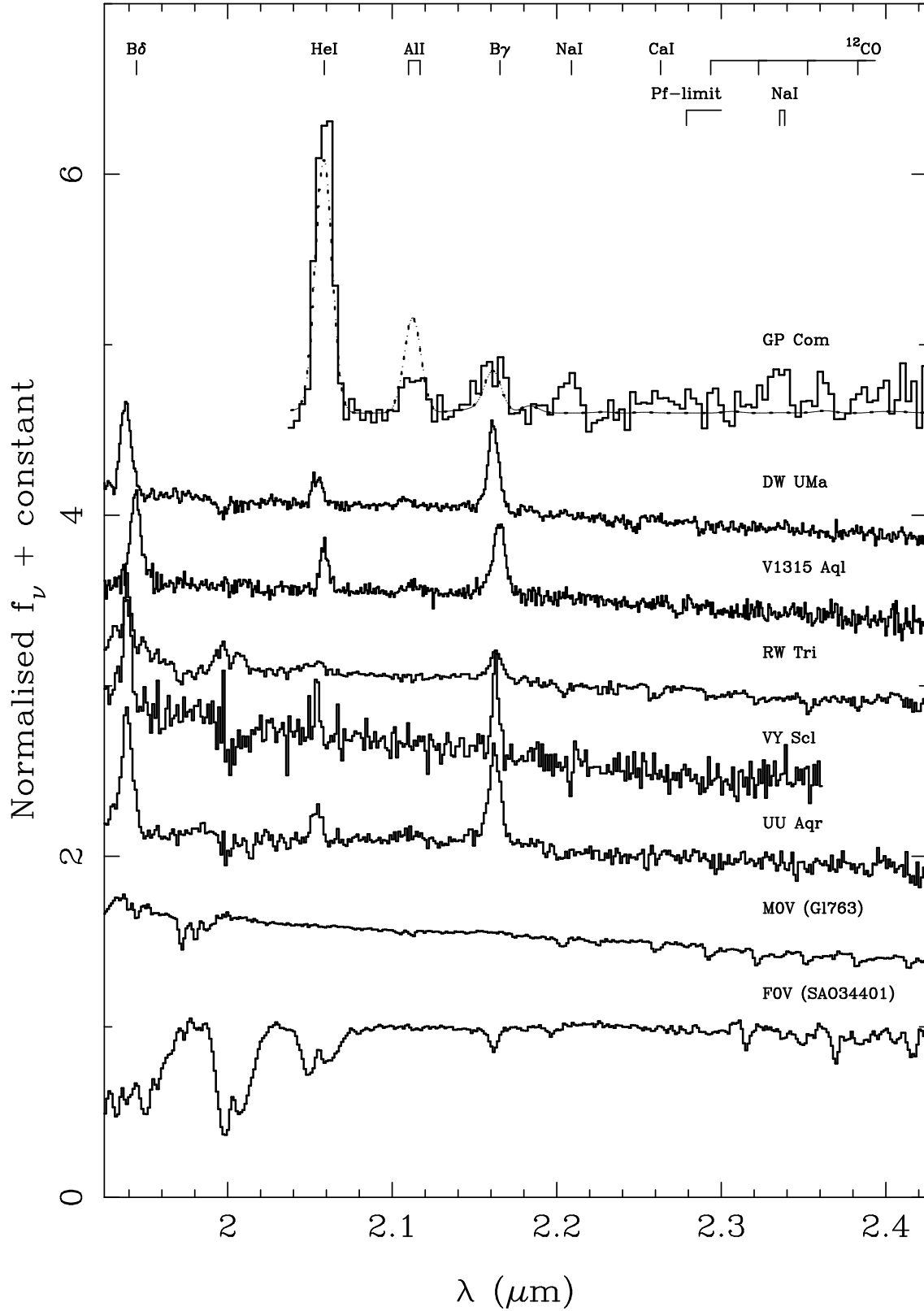


**Figure 2.** K-band spectra of the novalike variables GP Com, DW UMa, V1315 Aql, RW Tri, VY Scl, UU Aqr and an M0V star. The spectra have been normalised by dividing by the flux at 2.4  $\mu\text{m}$  and then offset by adding a multiple of 0.5 to each spectrum. Also shown is the spectrum of an F0V star, normalised by dividing by a spline fit to its continuum, which indicates the location of telluric absorption features; spectral features within the strongest absorption bands are highly uncertain. The dashed line under the spectrum of GP Com is a model spectrum from gas in LTE (see section 4.1 for details).

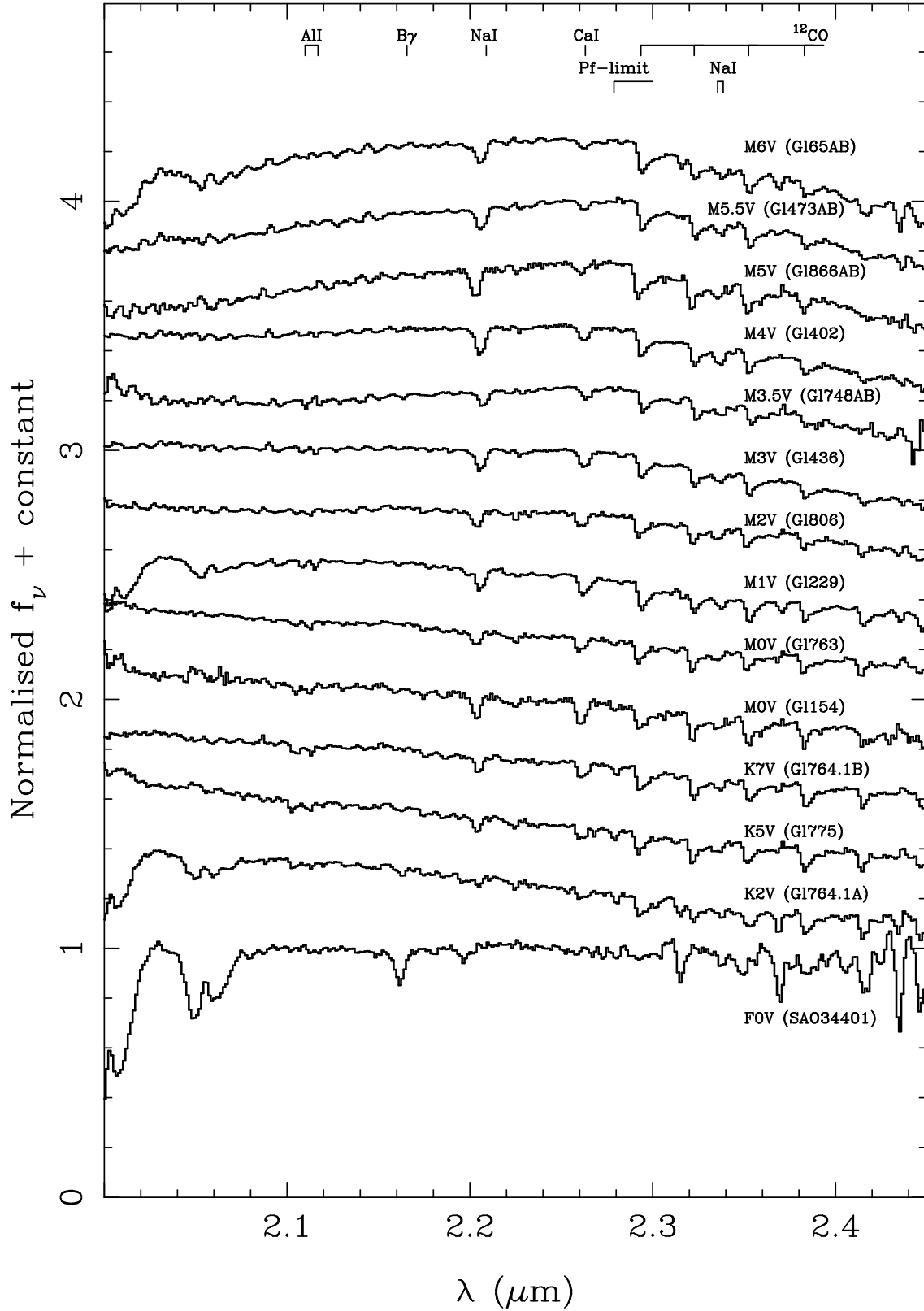


**Figure 3.** K-band spectra of K2V–M6V spectral-type template stars. The spectra have been normalised by dividing by the flux at 2.24  $\mu\text{m}$  and then offset by adding a multiple of 0.25 to each spectrum. Also shown is the spectrum of an F0V star, normalised by dividing by a spline fit to its continuum, which indicates the location of telluric absorption features; spectral features within the strongest absorption bands are highly uncertain.

**Table 1.** Journal of observations. The classifications and orbital periods of the CVs have been taken from the catalogue of Ritter & Kolb (1998). The spectral types of the late-type dwarfs have been taken from the catalogue of Kirkpatrick, Henry & McCarthy (1991), unless otherwise noted. Note that the classification of BK Lyn as the first novalike variable below the period gap (Dobrzycka & Howell 1992) has been questioned by Ringwald et al. (1996), who speculate that the object may instead be a dwarf nova with rare outbursts akin to those observed in objects like WZ Sge. For the purposes of this paper, we have grouped BK Lyn with the dwarf novae below the period gap.

Cataclysmic variables						
Object	Class	Period (hours)	Date	UTC start	UTC end	Exposure time (seconds)
RW Tri	NL UX	5.57	21/10/95	08:30	09:05	1700
VY Scl	NL VY	3.99	21/10/95	07:37	08:18	1900
UU Aqr	NL UX	3.93	21/10/95	09:16	09:32	800
V1315 Aql	NL UX SW	3.35	08/09/95	07:54	08:05	480
DW UMa	NL UX SW	3.28	03/02/97	11:14	11:53	1920
BK Lyn	NL SH?	1.80	06/02/96	10:18	11:14	2880
GP Com	NL AC	0.78	08/02/93	15:39	16:10	1440
YZ Cnc	DN SU	2.08	05/02/96	07:20	11:34	12000
LY Hya	DN	1.80	05/02/96	13:14	15:32	6720
T Leo	DN SU	1.41	06/02/96	13:22	15:25	5760
SW UMa	DN SU DQ?	1.36	06/02/96	07:17	10:11	8160
WZ Sge	DN SU WZ CP	1.36	28/05/97	11:49	14:39	8640

Late-type dwarfs						
Object	Spectral type	Date	UTC start	UTC end	Exposure time (seconds)	
GL764.1A	K2V <sup>a</sup>	20/10/95	07:26	07:35	192	
GL775	K5V	20/10/95	06:20	06:27	96	
GL764.1B	K7V	20/10/95	05:43	05:52	240	
GL154	M0V <sup>b</sup>	21/10/95	09:39	09:48	192	
GL763	M0V	20/10/95	06:00	06:08	144	
GL229	M1V	06/02/96	05:00	05:08	72	
GL806	M2V	20/10/95	07:12	07:21	192	
GL436	M3V	05/02/96	11:56	12:06	192	
GL748AB	M3.5V	28/05/97	11:17	11:26	576	
GL402	M4V	05/02/96	11:41	11:46	120	
GL866AB	M5V	21/10/95	05:25	05:33	192	
GL473AB	M5.5V <sup>c</sup>	06/02/96	15:44	16:02	288	
GL65AB	M6V	05/02/96	05:14	05:22	192	

<sup>a</sup>Gliese (1969)

<sup>b</sup>Hawley, Gizis & Reid (1996)

<sup>c</sup>Henry, Kirkpatrick & Simons (1994)

equivalent widths and velocity widths of the most prominent spectral lines identified in figures 1, 2 and 3.

#### 4.1 Emission lines

The spectra of the dwarf novae below the period gap in figure 1 are dominated by strong emission lines of HeI and

the Paschen and Brackett series of H I. The large velocity and equivalent widths of these lines (see table 2) indicate an accretion disc origin. This conclusion is further supported by the double-peaked emission-line profiles exhibited by the high-inclination dwarf novae LY Hya and WZ Sge (see also Skidmore et al. 1999 and Mason et al. 1999) in figure 1.

With the exception of the double-degenerate system GP

Com, which will be discussed in more detail below, the spectra of the novalike variables in figure 2 are dominated by strong, single-peaked emission lines of H I (Brackett- $\gamma$  and Brackett- $\delta$ ) and He I (2.0587  $\mu\text{m}$ ). This is in stark contrast to what one might expect from standard accretion disc theory (e.g. Horne & Marsh 1986), which predicts that emission lines from high inclination discs, such as those in the eclipsing systems DW UMa, V1315 Aql, RW Tri and UU Aqr, should appear double peaked. The absence of double-peaked profiles in high-inclination novalikes is also observed in the optical (see Dhillon 1996) and is one of the defining characteristics of the so-called SW Sex stars, of which DW UMa, V1315 Aql and UU Aqr are members.

GP Com consists of a CO white dwarf and a helium degenerate star in an orbit of 46 min period. Neither star is directly visible – the optical light from the system is dominated by the accretion disc, which has a spectrum composed almost entirely of helium and nitrogen emission lines reflecting the products of hydrogen burning and CNO processing in the helium degenerate donor. A very simple model, based upon LTE emission from an  $\sim 11\,000$  K optically thin (in the continuum) slab, provides a surprisingly good fit to the optical spectrum of GP Com (Marsh, Horne & Rosen 1991). In figure 2, the same model has been applied to the IR spectrum of GP Com, with equally good results. The model predicts the existence of three strong emission lines in the K-band, all of He I, which are all present in the actual spectrum. Note that there is also some evidence for a fourth emission line in the spectrum at 2.2  $\mu\text{m}$ , apparently unrelated to any telluric features, that we have been unable to identify.

## 4.2 Absorption lines/bands

RW Tri is the only CV presented in figures 1 and 2 which shows absorption features from the secondary star – one can clearly make out the profiles of Al I, Na I, Ca I and  $^{12}\text{CO}$  in the spectrum. The distinctive water absorption band at  $\sim 2.3$   $\mu\text{m}$ , so prominent in the spectra of the late M-stars presented in figure 3, is absent in RW Tri, indicating that its secondary is most likely a late K-dwarf. In order to estimate the spectral type of the secondary star in RW Tri from our data, and to determine its contribution to the total K-band flux, we used an optimal subtraction technique (e.g. Dhillon & Marsh 1993). First, we normalised the spectra of RW Tri and the template stars by dividing by a third-order polynomial fit to the continuum. A constant times the normalised template spectrum was then subtracted from the normalised spectrum of RW Tri and the constant adjusted so as to minimise the residual scatter in regions containing secondary star features. The residual scatter is measured by carrying out the subtraction and then computing the  $\chi^2$ -value between the residual spectrum and a smoothed version of itself. Prior to the subtraction, the template spectra should be broadened to account for the rotational velocity of the secondary star; the low resolution of our data, however, made this step unnecessary. The value obtained for the percentage contribution naturally depends on spectral type – the correct spectral type being the one which minimises the value of  $\chi^2$ . Using this method we find that the secondary star contributes  $65 \pm 5\%$  (1- $\sigma$  error) of the K-band light in RW Tri and that the spectral type of the secondary star is M0V. This spectral-type determination is in good

agreement with the results of the skew mapping experiments of Smith, Cameron & Tucknott (1993), who derive a spectral type of K7V or cooler, and with the predictions of the main-sequence spectral type-period relationship of Smith & Dhillon (1998), which suggests a spectral type of K9V.

None of the other CVs show any signs of absorption features from the secondary star. In these cases it is possible to determine an upper limit to the contribution of the secondary star. This is done by subtracting a constant times the normalised template spectrum from the normalised CV spectrum, until spectral absorption features from the template star appear in emission in the CV spectrum. The value of the constant at this point represents an upper limit to the fractional contribution of the secondary star. The contribution found depends on the spectral type of the template used. As the spectral type of the secondary star is unknown for these systems, we used the period-spectral type relationship of Smith & Dhillon (1998) to select an appropriate spectral type for the template star. The spectral type used for each CV, along with the corresponding upper limits to the secondary star contribution, are listed in table 4.

It is seen that the secondary star contributes less than 30-55% for the novalikes and 10-30% for the dwarf novae below the period gap. Exceptions are VY Scl and LY Hya, where poor signal-to-noise has resulted in very high values – the significance of these results is that we would have to obtain better signal-to-noise if we are to have any hope of observing the secondary in these systems, regardless of its contribution to the K-band light. A further exception is WZ Sge, in which the secondary must contribute less than 10% of the K-band light. This is in agreement with Littlefair et al. (1999) who find that the secondary star in WZ Sge contributes less than 20% to the J-band light, and Ciardi et al. (1998) who model the near-IR flux in WZ Sge and find that the secondary is a cool ( $\sim 1700$  K) star which contributes approximately 10% of the overall IR flux.

## 4.3 Distances

The distances to CVs can be measured from K-band spectra using a modification of a method first proposed by Bailey (1981). The distance modulus can be rewritten in terms of the K-band surface brightness as

$$S_k = m_K + 5 - 5 \log d + 5 \log(R/R_\odot), \quad (1)$$

where  $m_K$  is the apparent K-band magnitude,  $d$  is the distance in parsecs and  $R$  is the radius of the star. For a star of one solar radius,  $S_k$  is equal to the absolute K-band magnitude. Since the radius of the secondary star is equal to the radius of the Roche lobe, the orbital period and mass of the secondary are sufficient to determine its radius (there is also a weak dependence on mass ratio).  $m_K$  is derived from the K-band magnitude of the CV and the percentage contribution of the secondary star. Given  $m_K$  and the value of  $S_k$ , which can be obtained from the  $V - K$  colour (or spectral type) of the secondary using the empirical calibrations derived from field dwarfs by Ramseyer (1994), it is possible to estimate the distance using the above equation. Note that the distances to only 5 of the surveyed CVs are estimated here, as the remaining 7 CVs do not have published K-band magnitudes.

#### 4.3.1 *RW Tri*

The K-band magnitude of RW Tri is 11.59 (Longmore et al. 1981). In conjunction with the percentage contribution estimated in section 4.2, this gives a K-band magnitude for the secondary star of  $m_K = 12.06 \pm 0.08$ . Assuming the error in  $S_k$  is dominated by the error in spectral type (estimated to be one spectral type sub-classification), Bessell (1991) gives a  $V - K$  colour for the secondary of  $V - K = 3.65 \pm 0.1$ . Using the calibrations in Ramseyer (1994) this gives  $S_k = 4.43 \pm 0.1$ . We have estimated the radius of the secondary to be  $R/R_\odot = (0.61 \pm 0.2)$  from the orbital period-radius relation (equation 11) given by Smith & Dhillon (1998). These values, in conjunction with equation 1 give a distance to RW Tri of  $d = 205 \pm 90$  parsecs. McArthur et al. (1999) used the Hubble Space Telescope to obtain a parallax for RW Tri, establishing the distance to RW Tri at  $341_{-38}^{+31}$  parsecs. The discrepancy in the two results may be due to the fact that the actual K-band magnitude of RW Tri at the time of our observation is unknown and we have had to adopt the value obtained by Longmore et al. (1981). We know, however, that there is a long-term variation in the V-band magnitude of RW Tri at primary minimum, ranging from 13.7 to 15.4, suggesting there is an uneclipsed, variable component (Longmore et al. 1981). One might expect to see variation on a similar scale in the K-band (the actual long-term K-band variation has never been recorded), in which case our results are consistent with distances ranging from 90–400 parsecs.

#### 4.3.2 *WZ Sge*

The K magnitude of WZ Sge is 13.3 (Ciardi et al. 1998), which in conjunction with our upper limit to the secondary star contribution implies that  $m_K \geq 15.8$ . Smak (1993) estimates the radius of the secondary to be  $R_2/R_\odot = 0.11$ . Determining  $S_k$  is more problematic. Ciardi et al. (1998) find evidence that the secondary in WZ Sge is very cool (less than 1700 K) and Littlefair et al. (1999) use distance estimates by Spruit & Rutten (1998) and Smak (1993) to constrain the spectral type of the secondary to be later than M7.5.  $S_k$  for M7.5 (from Bessell 1991) is 6.8 and we shall adopt this value. Using these values we obtain a distance to WZ Sge of  $d \geq 69$  parsecs. Spruit & Rutten (1998) and Smak (1993) both found a distance to WZ Sge of 48 parsecs by fitting white dwarf models to UV spectra of WZ Sge obtained using the HST and the IUE, respectively.

#### 4.3.3 *T Leo*

The K magnitude of T Leo is 14.01 (Sproats, Howell & Mason 1996), which implies  $m_K \geq 15.3$ . We have estimated the radius of the secondary from the orbital period-radius relation given by Smith & Dhillon (1998). Likewise,  $S_k$  follows from the data in Bessell (1991) and a spectral type estimated from the orbital period-spectral type relationship in Smith & Dhillon (1998). Using these values we find  $d \geq 120$  parsecs, close to the value of  $d \sim 100$  parsecs found by Howell et al. (1999).

#### 4.3.4 *YZ Cnc*

The K magnitude of YZ Cnc is 14.37 (Sherrington & Jameson 1983), which implies  $m_K \geq 16$ . Again, we estimate  $S_k$  and the radius of the secondary star from the orbital period and the relationships given by Smith & Dhillon (1998). We find  $d \geq 290$  parsecs. Patterson (1984) finds a distance to YZ Cnc of  $\sim 130$  parsecs, using a method based on the equivalent width of  $H\beta$  and the shape of the continuum. The large discrepancy between these numbers is almost certainly due to the relatively unreliable techniques which Patterson (1984) was forced to use.

#### 4.3.5 *BK Lyn*

The K magnitude of BK Lyn is 14.63 (Sproats, Howell & Mason 1996). Following the same method as for YZ Cnc and T Leo, we obtain  $d \geq 185$  parsecs. Note that Dobrzycka & Howell (1992) derived a value of  $d \sim 1000$  parsecs, but this was based upon the assumption that the absolute magnitude of BK Lyn is the same as that typically found for novalikes (i.e.  $M_V \sim +4$ ), and is hence highly uncertain.

### 4.4 Time resolved spectra

Time resolved spectra were obtained for T Leo, SW UMa, YZ Cnc and WZ Sge. Unfortunately, a combination of poor signal-to-noise and velocity resolution means that radial velocity studies and Doppler tomography were fruitless (with the exception of WZ Sge – see Skidmore et al. 1999 and Mason et al. 1999). Skew mapping (see Smith, Cameron & Tucknott 1993) was performed, but no systems showed signs of the secondary star. Equivalent width light curves were obtained for all stars, but only those of T Leo and YZ Cnc show significant features, and are described here.

#### 4.4.1 *YZ Cnc*

Figure 4 shows the equivalent width light curves for YZ Cnc. Both the Brackett lines and HeI show a modulation on the orbital period, with maximum light at  $\phi \sim 0.0$ . van Paradijs et al. (1994) find a similar modulation in the optical data, but with different phasing, with maximum light at  $\phi \sim 0.8$ . They attribute this to bright spot modulations. It is likely that the modulations we observe in the K-band share the same source, given that the discrepancy in phase is well within the error quoted for the ephemeris given by van Paradijs et al. (1994). The variation is not as marked in the K-band as in the optical, perhaps suggesting that the bright spot contributes relatively less light to the system in the IR.

The Paschen- $\alpha$  line in YZ Cnc shows unusual behaviour, but this line is strongly affected by telluric features and hence the data are uncertain.

#### 4.4.2 *T Leo*

Figure 5 shows the equivalent width light curves for T Leo. The data is of poorer time resolution and signal-to-noise than the YZ Cnc data of figure 4. Paschen- $\alpha$  and the Brackett lines appear to show a similar variation to that observed in YZ Cnc, with the exception that maximum light is now



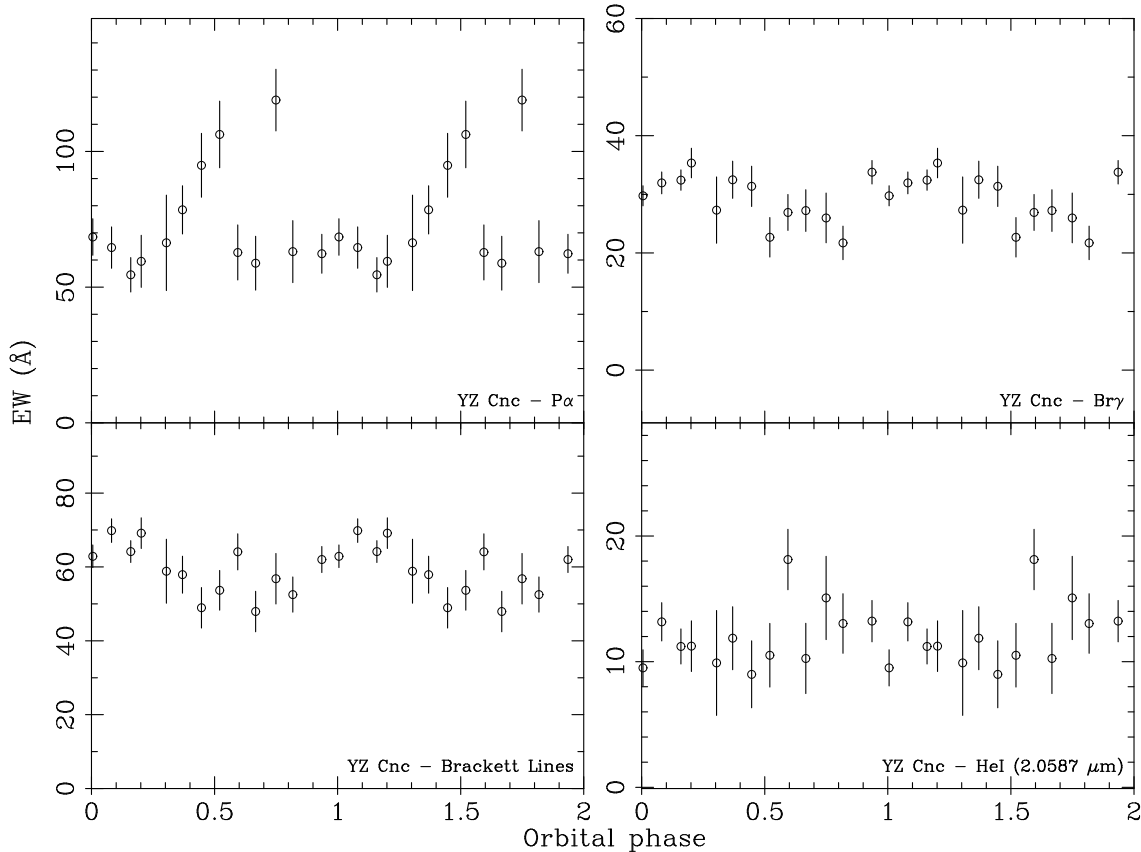


**Figure 4.** Equivalent width (EW) light curves of YZ Cnc. The light curves have been folded over two orbital cycles for clarity, according to the ephemeris of van Paradijs et al. (1994). Paschen- $\alpha$  was determined in the range 1.854–1.890  $\mu\text{m}$ , Brackett- $\gamma$  in the range 2.153–2.173  $\mu\text{m}$ , HeI in the range 2.053–2.062  $\mu\text{m}$  and the sum of the Brackett- $\gamma$  and Brackett- $\delta$  lines in the range 1.933–1.952 and 2.153–2.173  $\mu\text{m}$ .

located at  $\phi \sim 0.4$ . Phase should not be taken as reliable in this case as a considerable time has elapsed since the ephemeris of Shafter & Szkody (1984) was determined. We suggest that this variation may possibly be due to bright spot modulations, as in YZ Cnc, but poor signal-to-noise and errors in phasing make this conclusion uncertain. The HeI line does not show clear modulations with orbital phase.

## 5 DISCUSSION

The prospects of studying the secondary stars in novalike variables (particularly the SW Sex-type systems just above the period gap) and dwarf novae below the period gap appears bleak. With a few rare exceptions, the secondary star cannot even be detected, let alone studied. This, in turn, means that an essential tool in the study of the evolution of these systems – a knowledge of the mass and spectral type of the secondary star – is currently unavailable.

Why are the secondary stars so difficult to detect in these systems? In the case of the dwarf novae below the period gap, this is almost certainly due to the low surface temperature and small size of the secondary star, with the secondary contributing no more than 10–30% of the total K-band light. This compares with the easily detectable secondary stars in dwarf novae above the period gap, which typ-

ically contribute at least 75% of the K-band light (Dhillon & Marsh 1995).

Novalike variables also lie above the period gap, however, so why are their secondary stars not visible? One explanation is that the steady-state accretion discs in novalike variables are much brighter than the quiescent discs in dwarf novae of a similar orbital period; the resulting increase in shot noise from the disc spectrum overwhelms the weak signal from the secondary star. This does not explain, however, why the secondary star in DW UMa was not even visible during a 3–4 magnitude low-state (when accretion had virtually ceased) in the I-band spectra of Marsh & Dhillon (1997). This observation implies that the secondary star in DW UMa has an apparent magnitude of  $I > 19.5$  and hence a distance of at least  $\sim 850$  pc if the secondary star has spectral type M4.\* If this lower-limit to the distance is typical of most novalikes (or specifically, SW Sex stars), then it means that the mass transfer rates derived from techniques such as eclipse mapping (e.g. Rutten, van Paradijs & Tinbergen 1992) are underestimating the true values.

## ACKNOWLEDGEMENTS

We would like to thank Simon Duck and Lee Sproats for their help with putting together the various observing proposals which led to the award of telescope time for this

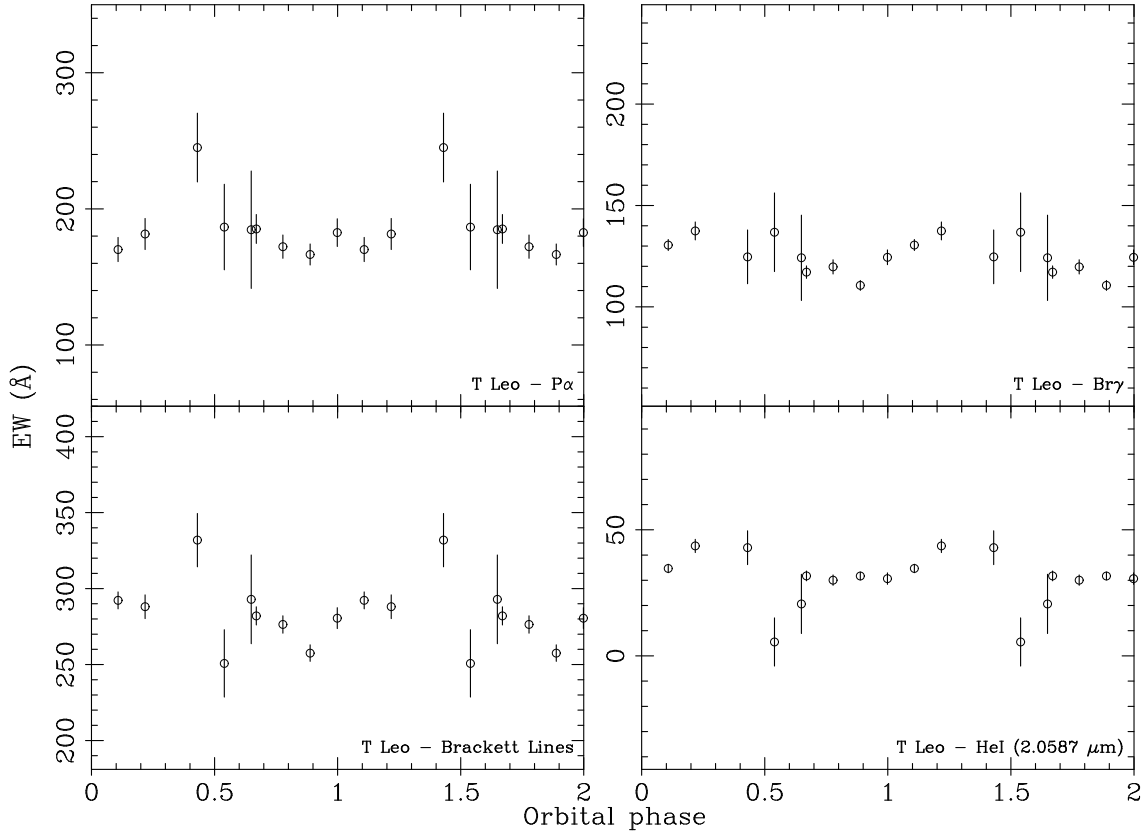


**Figure 5.** Equivalent width (EW) light curves of T Leo. The light curves have been folded over two orbital cycles for clarity, according to the ephemeris of Shafter & Szkody (1984). Paschen- $\alpha$  was determined in the range 1.854–1.890  $\mu\text{m}$ , Brackett- $\gamma$  in the range 2.153–2.173  $\mu\text{m}$ , HeI in the range 2.053–2.062  $\mu\text{m}$  and the sum of the Brackett- $\gamma$  and Brackett- $\delta$  lines in the range 1.933–1.952 and 2.153–2.173  $\mu\text{m}$ .

survey. We would also like to thank Tariq Shahbaz for his comments on this paper. UKIRT is operated by the Joint Astronomy Centre on behalf of the Particle Physics and Astronomy Research Council. The spectra of V1315 Aql and DW UMa were obtained through the UKIRT service programme. The data reduction and analysis were performed at the Sheffield node of the UK STARLINK computer network. SBH would like to acknowledge partial support of this work by NASA grants NAG5-4233 and GFSC-070.

## REFERENCES

- Bailey J. A., 1981, *MNRAS*, 197, 31  
 Bessell M. S., 1991, *AJ*, 101, 662  
 Ciardi D. R., Howell S. B., Hauschildt P. H., Allard F., 1998, *ApJ*, 504, 450  
 Daley P. N., Beard S. M., 1994, *Starlink User Note* 27, RAL  
 Dhillon V. S., Marsh T. R., 1993, in Regev O., Shaviv G., eds, *Cataclysmic Variables and Related Physics*. Inst. Phys. Publ., Bristol, p. 34  
 Dhillon V. S., Marsh T. R., 1995, *MNRAS*, 275, 89  
 Dhillon V. S., Marsh T. R., Duck S. R., Rosen S. R., 1997, *MNRAS*, 285, 95  
 Dhillon V. S., 1996, in Evans A., Wood J. H., eds, *Cataclysmic Variables and Related Objects*. Kluwer Academic Publishers, Dordrecht, p. 3  
 Dhillon V. S., 1998, in Howell S. B., Kuulkers E., Woodward C., eds, *Wild Stars in the Old West: Proceedings of the 13th North American Workshop on Cataclysmic Variables and Related Objects* (ASP Conference Series, Vol. 137). Astronomical Society of the Pacific, San Francisco, p. 23  
 Dobrzycka D., Howell S. B., 1992, *ApJ*, 388, 614  
 Friend M. T., Martin J. S., Smith R. C., Jones D. H. P., 1988, *MNRAS*, 233, 451  
 Gliese W., 1969, *Vöroff. Astr. Rechen-Inst. Heidelberg.*, No. 22  
 Hawley S. L., Gizis J. E., Reid I. N., 1996, *AJ*, 112, 2799  
 Henry T. J., Kirkpatrick J. D., Simons D. A., 1994, *AJ*, 108, 1437  
 Horne K., Marsh T. R., 1986, *MNRAS*, 218, 761  
 Horne K., 1986, *PASP*, 98, 609  
 Howell S. B., Ciardi D. R., Szkody P., van Paradijs J., Kuulkers E., Cash J., Sirk M., Long K. S., 1999, *PASP*, 111, 342  
 Joyce R. R., 1992, in Howell S. B., ed, *Astronomical CCD Observing and Reduction Techniques*. ASP Conference Series, Volume 23, p. 258  
 Kirkpatrick J. D., Henry T. J., McCarthy D. W. J., 1991, *ApJS*, 77, 417  
 Littlefair S. P., Dhillon V. S., Howell S. B., Ciardi D. R., 1999, *MNRAS*, in press  
 Longmore A. J., Lee T. J., Allen D. A., Adams D. J., 1981, *MNRAS*, 195, 825  
 Marsh T. R., Dhillon V. S., 1997, *MNRAS*, 292, 385  
 Marsh T. R., Horne K., Rosen S. R., 1991, *ApJ*, 366, 535  
 Mason E., Skidmore W., Howell S. B., Ciardi D. R., Littlefair S. P., Dhillon V. S., 1999, *MNRAS*, submitted  
 McArthur B. E. et al., 1999, *ApJ*, 520, 59  
 Patterson J., 1984, *ApJS*, 54, 443  
 Ramsay S. K., Mountain C. M., Geballe T. R., 1992, *MNRAS*, 259, 751

- Ramseyer T. F., 1994, ApJ, 425, 243  
Ringwald F. A., Thorstensen J. R., Honeycutt R. K.,  
Robertson J. W., 1996, MNRAS, 278, 125  
Ritter H., Kolb U., 1998, A&AS, 129, 83  
Rutten R. G. M., van Paradijs J., Tinbergen J., 1992, AA, 260,  
213  
Shafter A. W., Szkody P., 1984, ApJ, 276, 305  
Sherrington M. R., Jameson R. F., 1983, MNRAS, 205, 265  
Skidmore W., Mason E., Howell S. B., Ciardi D. R.,  
Littlefair S. P., Dhillon V. S., 1999, MNRAS, submitted  
Smak J., 1993, Acta Astronomica, 43, 101  
Smith D. A., Dhillon V. S., 1998, MNRAS, 301, 767  
Smith R. C., Cameron A., Tucknott D. S., 1993, in Regev O.,  
Shaviv G., eds, Cataclysmic Variables and Related Physics.  
Inst. Phys. Publ., Bristol, p. 70  
Smith R. C., Sarna M. J., Catalan M. S., Jones D. H. P., 1997,  
MNRAS, 287, 271  
Sproats L. N., Howell S. B., Mason K. O., 1996, MNRAS, 282,  
1211  
Spruit H. C., Rutten R. G. M., 1998, MNRAS, 299, 768  
van Paradijs J. et al., 1994, MNRAS, 267, 465  
Warner B., 1995, Cataclysmic Variable Stars. Cambridge  
University Press, Cambridge

**Table 2.** Wavelengths, equivalent widths and velocity widths of the most prominent lines visible in the IR spectra of the surveyed CVs. The line identifications have been based upon the list presented by Dhillon & Marsh (1995) and references therein. The wavelengths given for the  $^{12}\text{CO}$  lines refer to the band-heads. The vertical bars following lines of similar wavelength indicate that the equivalent width measurements apply to the entire blend. The two-letter codes indicate that a line was either not present (np) or present but not measurable (nm).

Line	$\lambda$ $\mu\text{m}$	VY Scl			EW Å	RW Tri			EW Å	UU Aqr			EW Å	LY Hya			EW Å	YZ Cnc		
		FWHM $\text{kms}^{-1}$	FWZI $\text{kms}^{-1}$			FWHM $\text{kms}^{-1}$	FWZI $\text{kms}^{-1}$			FWHM $\text{kms}^{-1}$	FWZI $\text{kms}^{-1}$			FWHM $\text{kms}^{-1}$	FWZI $\text{kms}^{-1}$			FWHM $\text{kms}^{-1}$	FWZI $\text{kms}^{-1}$	
B- $\epsilon$	1.8174	nm	nm	nm	nm	nm	nm	nm	nm	nm	nm	nm	nm	3000 $\pm$ 1000	nm	nm	1050 $\pm$ 100	nm		
P- $\alpha$	1.8751	nm	nm	nm	nm	nm	nm	nm	nm	nm	nm	170 $\pm$ 20	2200 $\pm$ 150	5200 $\pm$ 400	37 $\pm$ 4	900 $\pm$ 100	2200 $\pm$ 200			
B- $\delta$	1.9446	42 $\pm$ 5	800 $\pm$ 80	2600 $\pm$ 400	nm	nm	nm	42 $\pm$ 5	940 $\pm$ 90	3200 $\pm$ 400	94 $\pm$ 8	1800 $\pm$ 100	5900 $\pm$ 500	22 $\pm$ 2	960 $\pm$ 90	2500 $\pm$ 200				
HeI	2.0587	6 $\pm$ 2	380 $\pm$ 50	1100 $\pm$ 200	4 $\pm$ 1	750 $\pm$ 200	1300 $\pm$ 400	7 $\pm$ 2	730 $\pm$ 70	1300 $\pm$ 400	34 $\pm$ 5	1400 $\pm$ 100	2900 $\pm$ 400	9 $\pm$ 1	710 $\pm$ 70	2200 $\pm$ 200				
B- $\gamma$	2.1655	27 $\pm$ 4	730 $\pm$ 70	1500 $\pm$ 200	16 $\pm$ 1	1100 $\pm$ 300	2000 $\pm$ 400	56 $\pm$ 2	930 $\pm$ 90	2800 $\pm$ 200	103 $\pm$ 6	2200 $\pm$ 100	3900 $\pm$ 200	36 $\pm$ 1	1200 $\pm$ 100	3000 $\pm$ 400				
AlI	2.1099	np	np	np	nm	nm	nm	np	np	np	np	np	np	np	np	np				
AlI	2.1170	np	np	np	nm	nm	nm	np	np	np	np	np	np	np	np	np				
NaI	2.2062	np	np	np	-2.8 $\pm$ 0.5	nm	nm	np	np	np	np	np	np	np	np	np				
NaI	2.2090																			
CaI	2.2614																			
CaI	2.2631	np	np	np	-1.9 $\pm$ 0.9	nm	nm	np	np	np	np	np	np	np	np	np				
CaI	2.2657																			
$^{12}\text{CO}$	2.2935	np	np	np	-2 $\pm$ 1	nm	nm	np	np	np	np	np	np	np	np	np				
$^{12}\text{CO}$	2.3227																			
NaI	2.3355	np	np	np	-5 $\pm$ 1	nm	nm	np	np	np	np	np	np	np	np	np				
NaI	2.3386																			
$^{12}\text{CO}$	2.3525	np	np	np	-7 $\pm$ 1	nm	nm	np	np	np	np	np	np	np	np	np				
$^{12}\text{CO}$	2.3830	np	np	np	-2 $\pm$ 1	nm	nm	np	np	np	np	np	np	np	np	np				

Line	$\lambda$ $\mu\text{m}$	SW UMa			EW Å	T Leo			EW Å	BK Lyn			EW Å	WZ Sge		
		FWHM $\text{kms}^{-1}$	FWZI $\text{kms}^{-1}$			FWHM $\text{kms}^{-1}$	FWZI $\text{kms}^{-1}$			FWHM $\text{kms}^{-1}$	FWZI $\text{kms}^{-1}$			FWHM $\text{kms}^{-1}$	FWZI $\text{kms}^{-1}$	
B- $\epsilon$	1.8174	nm	1600 $\pm$ 200	nm	nm	1200 $\pm$ 200	nm	nm	nm	600 $\pm$ 200	nm	nm	nm	nm	nm	
P- $\alpha$	1.8751	244 $\pm$ 9	1300 $\pm$ 100	4500 $\pm$ 200	157 $\pm$ 6	1600 $\pm$ 100	3700 $\pm$ 200	30 $\pm$ 5	800 $\pm$ 80	1900 $\pm$ 200	nm	nm	nm	nm	nm	
B- $\delta$	1.9446	128 $\pm$ 5	1300 $\pm$ 100	2300 $\pm$ 200	93 $\pm$ 3	1300 $\pm$ 100	4000 $\pm$ 200	18 $\pm$ 3	850 $\pm$ 80	1800 $\pm$ 200	nm	nm	nm	nm	nm	
HeI	2.0587	34 $\pm$ 3	920 $\pm$ 90	2000 $\pm$ 200	32 $\pm$ 2	980 $\pm$ 90	2300 $\pm$ 200	5 $\pm$ 2	580 $\pm$ 50	2200 $\pm$ 400	26 $\pm$ 1	1600 $\pm$ 100	3800 $\pm$ 200			
B- $\gamma$	2.1655	147 $\pm$ 4	1400 $\pm$ 100	3500 $\pm$ 200	119 $\pm$ 2	1400 $\pm$ 100	3500 $\pm$ 200	21 $\pm$ 2	920 $\pm$ 150	2900 $\pm$ 200	80 $\pm$ 1	2200 $\pm$ 150	3400 $\pm$ 200			
AlI	2.1099	np	np	np	np	np	np	np	np	np	nm	nm	nm			
AlI	2.1170	np	np	np	np	np	np	np	np	np	nm	nm	nm			
NaI	2.2062	np	np	np	np	np	np	np	np	np	nm	nm	nm			
NaI	2.2090										nm	nm	nm			
CaI	2.2614															
CaI	2.2631	np	np	np	np	np	np	np	np	np	nm	nm	nm			
CaI	2.2657															
$^{12}\text{CO}$	2.2935	np	np	np	np	np	np	np	np	np	nm	nm	nm			
$^{12}\text{CO}$	2.3227															
NaI	2.3355	np	np	np	np	np	np	np	np	np	nm	nm	nm			
NaI	2.3386															
$^{12}\text{CO}$	2.3525	np	np	np	np	np	np	np	np	np	nm	nm	nm			
$^{12}\text{CO}$	2.3830	np	np	np	np	np	np	np	np	np	nm	nm	nm			

Line	$\lambda$ $\mu\text{m}$	DW UMa			EW Å	V1315 Aql			EW Å	GP Com		
		FWHM $\text{kms}^{-1}$	FWZI $\text{kms}^{-1}$			FWHM $\text{kms}^{-1}$	FWZI $\text{kms}^{-1}$			FWHM $\text{kms}^{-1}$	FWZI $\text{kms}^{-1}$	
B- $\epsilon$	1.8174	nm	nm	nm	nm	nm	nm	nm	nm	nm	nm	
P- $\alpha$	1.8751	79 $\pm$ 3	850 $\pm$ 30	1900 $\pm$ 160	61 $\pm$ 8	1200 $\pm$ 100	3400 $\pm$ 200	nm	nm	nm	nm	
B- $\delta$	1.9446	31 $\pm$ 1	930 $\pm$ 150	2200 $\pm$ 200	32 $\pm$ 2	1100 $\pm$ 100	2200 $\pm$ 200	nm	nm	nm	nm	
HeI	2.0587	7 $\pm$ 1	730 $\pm$ 50	1800 $\pm$ 200	11 $\pm$ 1	820 $\pm$ 80	1600 $\pm$ 200	200 $\pm$ 7	1660 $\pm$ 70	4100 $\pm$ 150		
B- $\gamma$	2.1655	44 $\pm$ 1	1130 $\pm$ 20	3200 $\pm$ 150	46 $\pm$ 1	1400 $\pm$ 50	2600 $\pm$ 200	51 $\pm$ 7	2600 $\pm$ 400	4400 $\pm$ 400		
AlI	2.1099	np	np	np	np	np	np	np	np	np	np	
AlI	2.1170	np	np	np	np	np	np	np	np	np	np	
NaI	2.2062	np	np	np	np	np	np	np	np	np	np	
NaI	2.2090											
CaI	2.2614											
CaI	2.2631	np	np	np	np	np	np	np	np	np	np	
CaI	2.2657											
$^{12}\text{CO}$	2.2935	np	np	np	np	np	np	np	np	np	np	
$^{12}\text{CO}$	2.3227											
NaI	2.3355	np	np	np	np	np	np	np	np	np	np	
NaI	2.3386											
$^{12}\text{CO}$	2.3525	np	np	np	np	np	np	np	np	np	np	
$^{12}\text{CO}$	2.3830	np	np	np	np	np	np	np	np	np	np	

**Table 3.** Wavelengths and equivalent widths (in Ångstroms) of the most prominent lines visible in the IR spectra of the surveyed dwarf stars. The line identifications have been based upon the list presented by Dhillon & Marsh (1995) and references therein. The wavelengths given for the  $^{12}\text{CO}$  lines refer to the band-heads. Equivalent widths for the  $\text{H}_2\text{O}$  band were measured between 2.29 and 2.44  $\mu\text{m}$ . The vertical bars following lines of similar wavelength indicate that the equivalent width measurements apply to the entire blend. The two-letter codes indicate that a line was either not present (np) or present but not measurable (nm). Note that the values indicated by asterisks are subject to unknown systematic errors due to difficulties in continuum normalisation.

Line	$\lambda$ ( $\mu\text{m}$ )	G1764.1A K2V	G1775 K5V	G1764.1B K7V	G1154 M0V	G1763 M0V	G1229 M1V	G1806 M2V	G1436 M3V	G1748AB M3.5V	G1402 M4V	G1866AB M5V	G1473AB M5.5V	G165AB M6V
AlI 2.1099		nm	-4.3 $\pm$ 0.5	-3.7 $\pm$ 0.6	-3.1 $\pm$ 0.6	-2.1 $\pm$ 0.4	-1.3 $\pm$ 0.3	-1.3 $\pm$ 0.4	-0.8 $\pm$ 0.4	nm	nm	nm	nm	nm
AlI 2.1170														
NaI 2.2062		nm	-2.1 $\pm$ 0.4	-2.9 $\pm$ 0.4	-3.2 $\pm$ 0.6	-3.0 $\pm$ 0.3	-4.2 $\pm$ 0.4	-3.8 $\pm$ 0.4	-4.9 $\pm$ 0.4	-3.1 $\pm$ 0.4	-6.7 $\pm$ 0.5	-6.6 $\pm$ 0.6	-5.8 $\pm$ 0.3	-6.5 $\pm$ 0.4
NaI 2.2090														
CaI 2.2614														
CaI 2.2631		-1.2 $\pm$ 0.4	-2.9 $\pm$ 0.4	-3.1 $\pm$ 0.5	-3.5 $\pm$ 0.5	-2.9 $\pm$ 0.5	-6.4 $\pm$ 0.4	-4.4 $\pm$ 0.4	-4.3 $\pm$ 0.4	-2.9 $\pm$ 0.4	-4.6 $\pm$ 0.5	-6.0 $\pm$ 0.7	-3.5 $\pm$ 0.3	-2.3 $\pm$ 0.3
CaI 2.2657														
H <sub>2</sub> O 2.2900		-26 $\pm$ 2	-35 $\pm$ 2	-80 $\pm$ 2	-61 $\pm$ 3	-62 $\pm$ 2	-72 $\pm$ 2*	-152 $\pm$ 2	-194 $\pm$ 1	-222 $\pm$ 2	-249 $\pm$ 2	-346 $\pm$ 2	-315 $\pm$ 1	-235 $\pm$ 2
$^{12}\text{CO}$ 2.2935		-3.3 $\pm$ 0.6	-1.9 $\pm$ 0.6	-3.6 $\pm$ 0.6	-9 $\pm$ 1	-3.1 $\pm$ 0.7	-16 $\pm$ 1*	-3.9 $\pm$ 0.6	-2.0 $\pm$ 0.6	-3.8 $\pm$ 0.5	-4 $\pm$ 1	-6.1 $\pm$ 0.8	-4.0 $\pm$ 0.4	-3.9 $\pm$ 0.5
$^{12}\text{CO}$ 2.3227														
NaI 2.3355		-4 $\pm$ 1	-5.1 $\pm$ 0.7	-6.5 $\pm$ 0.8	-14 $\pm$ 1	-4.8 $\pm$ 0.9	-20 $\pm$ 1*	-7.2 $\pm$ 0.8	-6.9 $\pm$ 0.7	-9.0 $\pm$ 0.7	-11 $\pm$ 1	-12 $\pm$ 1	-9.8 $\pm$ 0.6	-8.7 $\pm$ 0.6
NaI 2.3386														
$^{12}\text{CO}$ 2.3525		-2.0 $\pm$ 0.8	-4.4 $\pm$ 0.8	-4.1 $\pm$ 0.9	-14 $\pm$ 1	-1.6 $\pm$ 0.9	-18 $\pm$ 1*	-3.1 $\pm$ 0.8	-4.7 $\pm$ 0.7	-5.2 $\pm$ 0.7	-5 $\pm$ 1	-7.5 $\pm$ 1	-6.1 $\pm$ 0.6	-5.5 $\pm$ 0.8
$^{12}\text{CO}$ 2.3830		-0.5 $\pm$ 0.9	-2.4 $\pm$ 0.8	-2 $\pm$ 1	-11 $\pm$ 1	-1.5 $\pm$ 0.8	-11 $\pm$ 1*	-1.6 $\pm$ 0.7	-3.5 $\pm$ 0.7	-2.0 $\pm$ 0.8	-2 $\pm$ 1	-1.2 $\pm$ 0.9	-2.1 $\pm$ 0.5	-1.2 $\pm$ 0.6

**Table 4.** Upper limits to the contributions of the secondary star to the total K-band flux.

Object	Secondary star contribution	Error	Spectral-type template used
VY Scl	90%	10%	M4V
DW UMa	35%	5%	M4V
V1315 Aql	30%	5%	M4V
UU Aqr	55%	5%	M4V
BK Lyn	50%	5%	M5V
LY Hya	100%	10%	M5V
YZ Cnc	20%	5%	M5V
SW UMa	20%	5%	M5.5V
T Leo	30%	5%	M5.5V
WZ Sge	10%	5%	M5.5V